Macromolecules

pubs.acs.org/Macromolecules Article

Modulating the Contact Angle between Nonpolar Polymers and SiO_2 Nanoparticles

Anirban Majumder, Anne N. Radzanowski, Ching-Yu Wang, Yijiang Mu, E. Bryan Coughlin, Raymond J. Gorte, John M. Vohs, and Daeyeon Lee*

Cite This: *Macromolecules* 2024, 57, 8554–8561 Read Online

ACCESS | Metrics & More | Article Recommendations | Supporting Information

ABSTRACT: Polymer–nanoparticle interactions play an important role in determining the morphology and properties of polymer nanocomposites and controlling the polymeric reactions involving heterogeneous catalysts. Here, we modulate the interactions between nonpolar polymers and nanoparticles by modifying the nanoparticle surface chemistry and quantify the interaction strength through direct contact angle measurements. We investigate the interactions of three nonpolar polymers, polystyrene, polyethylene, and polycyclooctene, with silica nanoparticles whose surface chemistry has been modified by atomic layer deposition of titania and calcium carbonate and by alkyl silanization. Significant differences in polymer–nanoparticle interactions are observed, which can be attributed to differences in the polarizability of the polymers and oxide surface composition. Compared to fully hydrogenated polycyclooctene, polycyclooctene is shown to have stronger interactions with most metal oxides; however, this trend is reversed following alkyl silanization of the silica nanoparticles, which makes the surface of the particles less polar. These differences in interactions can be leveraged to make polymer nanocomposites with unique properties and enable the selective conversion of polymers without the need for separations.

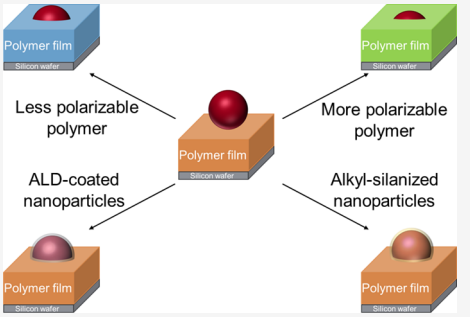

1. INTRODUCTION

Understanding and controlling the interactions between polymers and nanoparticles are key to designing new materials and processes with desirable features and efficiency. Incorporating nanoparticles into a polymer matrix enables the fabrication of polymer nanocomposites with enhanced mechanical, optical, and transport properties.[1−3] Strong interactions between the polymer and nanoparticles facilitate nanoparticle dispersion and strengthen the interface, leading to enhancement of the mechanical properties in the resulting nanocomposites.[4] Conversely, unfavorable interactions between polymers and nanoparticles can complicate processing and compromise the properties of nanocomposites due to nanoparticle aggregation.[5−7]

The need for understanding and modulating these interactions is not limited to polymer nanocomposites. Polymer–nanoparticle interactions are of great importance in polymeric reactions that use heterogeneous catalysts.[8] These catalysts often consist of an active component supported on a porous oxide support that has nanopores for achieving high surface areas. For polymers to undergo a reaction, they must infiltrate into these nanopores[9,10] in a process that is heavily influenced by interactions between the polymer chains and the pore surface. Interactions between the pore surface and product molecules from the reactions are also important. Strong interactions between the product and surface may inhibit new reactant molecules from interacting with the surface, significantly reducing the reactivity of the system. Differential interactions among polymers and the nanoparticle surface can also facilitate the selective conversion of polymers from complex feed streams that are often present in polymer waste.

Despite its importance, the strength of polymer–nanoparticle interactions is often described using qualitative terms such as "weakly interacting", "neutrally interacting", or "strongly interacting" based on the chemical structures of the polymer and the nanoparticle and possible modes of interactions between the two.[3,11−14] Such descriptors, while offering a rudimentary understanding, fall short of providing the precise quantification necessary for the systematic design and optimization of processes involving polymers and nanoparticles. Furthermore, although the interactions between polymers with polar functional groups and nanoparticles, which may engage in specific interactions, can be qualitatively assessed, a significant gap in understanding exists regarding the quantification and control of interactions between nonpolar polymers and nanoparticles. Predictions of the interaction

Received: April 11, 2024
Revised: August 8, 2024
Accepted: August 8, 2024
Published: August 20, 2024

https://doi.org/10.1021/acs.macromol.4c00823
Macromolecules 2024, 57, 8554–8561

strength between nonpolar polymers and inorganic surfaces of different chemistry (e.g., SiO_2 vs TiO_2) are not well understood. Given that most commodity polymers consist of nonpolar units, this lack of insight poses a substantial barrier to progress in fields that demand detailed knowledge and adjustment of polymer−nanoparticle interactions.

An effective strategy to bridge this gap is through measurement of the polymer−nanoparticle contact angle, offering a quantitative measure of these interactions that rely on various factors. Efforts to measure polymer−solid surface contact angle have been made by using different approaches. The polymer−nanoparticle contact angles have been calculated by modeling the infiltration dynamics of polymers into dense packings of nanoparticles using the Lucas−Washburn equation[15,16]

$$d^2 = \left(\frac{\gamma R_{\text{pore}} \cos\theta}{4\eta\tau^2}\right) t \tag{1}$$

where d is the depth of polymer infiltration into the nanoparticle packing, γ is the surface tension of the polymer, R_{pore} is the pore radius, θ is the equilibrium contact angle between the polymer and pore surface (or nanoparticle surface), η is the polymer melt viscosity, τ is the tortuosity of the packing, and t is the infiltration time. Polymers having lower contact angles exhibit faster infiltration rates within nanoparticle packings. However, several assumptions must be made for determining the contact angle with this approach. For example, one needs to assume a reference contact angle value for a polymer−nanoparticle pair with a known infiltration time to predict contact angles for other polymer−nanoparticle pairs. In a different study, the contact angle of polystyrene (PS) on a planar silica surface was determined by spin-coating an ultrathin polymer film onto the substrate and heating it above its glass-transition temperature to induce dewetting and the formation of sessile nanodroplets.[17] Through atomic force microscopy (AFM), researchers analyzed the nanodroplets' morphology, measuring the slope at the three-phase contact line and fitting the droplet shape to a spherical cap model to ascertain the polymer's contact angle on silica. However, this technique can only be used to measure polymer−solid contact angles below 90°. Also, this technique needs a planar solid surface and cannot be used for the determination of the contact angle of polymers on nanoparticles.

In the present study, we modulate the interactions between nonpolar polymers and nanoparticles by modifying the particle's surface chemistry and then quantify the interactions through direct contact angle measurement.[18,19] We use three nonpolar polymers of varying polarizabilities: polyethylene (PE), PS, and polycyclooctene (PCOE). While PE and PS are commodity polymers that are widely used, PCOE serves as a model polymer for partially dehydrogenated PE, an example of an upcycled polymer.[20,21] The C=C bonds in partially dehydrogenated PE can be functionalized with different functional groups to make valuable specialty polymers. To determine the contact angle, we placed spherical nanoparticles on top of polymer films and allowed them to equilibrate at the polymer−air interface by heating PS above its glass-transition temperature and heating PCOE and PE above their melting points. After equilibration, the height of the nanoparticles above the polymer−air interface was measured by AFM to determine the equilibrium polymer−nanoparticle contact angle.

To understand how the surface chemistry of nanoparticles affects the strength of interactions between nanoparticles and the polymer, we modified SiO_2 nanoparticles using atomic layer deposition (ALD) to coat the nanoparticles with various metal oxides and by alkyl silanization of the surface of the nanoparticles. We found that polarizability of the polymers is an important factor in determining their strength of interaction with different nanoparticle surfaces, and small differences in polarizability between polymers, for example, between PCOE and fully hydrogenated PCOE (hPCOE), can lead to significant differences in interaction strengths with nanoparticles. Quantifying the varying interaction strengths will enable the prudent design of polymer nanocomposites with desired morphologies and the design of heterogeneous catalysts that could facilitate the selective and efficient conversion of plastic waste.

2. EXPERIMENTAL SECTION

2.1. Materials. PS with a molecular weight of 88,000 g/mol ($Đ$ = 1.1) and PE with a molecular weight of 78,000 g/mol ($Đ$ = 1.05) were purchased from Polymer Source. PCOE was synthesized by the ring-opening metathesis polymerization of cis-cyclooctene ($M_{n,GPC}$ = 52,000 g/mol, $Đ$ = 1.62) following adapted ROMP procedures.[22,23] hPCOE was synthesized by hydrogenation of PCOE via a diimide reduction as adapted from the literature.[24,25] Full synthetic details and characterization can be found in the Supporting Information. Tetraethyl orthosilicate (TEOS) (reagent grade, 98%) was purchased from Sigma-Aldrich. Ammonium hydroxide was purchased from Fisher Chemical. Single-side polished silicon wafers were purchased from University Wafer. Titanium chloride ($TiCl_4$) and bis(2,2,6,6-tetra-methyl-3,5-heptanedionato) calcium ($Ca(TMHD)_2$) were purchased from Strem Chemicals, Inc. OTS was purchased from Sigma-Aldrich.

2.2. Synthesis and Characterization of Silica Nanoparticles. Silica nanoparticles were synthesized using the Stöber solution method.[26] In this procedure, 35 mL of ethanol 200 proof from Decon Laboratories and 2.8 mL of deionized water were added to a 50 mL glass bottle with a magnetic stir bar. Next, 1 mL of ammonium hydroxide was added, and the mixture was stirred for 1 min. Finally, 2.1 mL of TEOS was added and stirred overnight. This led to the formation of silica nanoparticles with an average diameter of approximately 230 nm. After the synthesis, particles were centrifuged, washed, and dispersed in deionized water for storage. Dynamic light scattering (DLS) and scanning electron microscopy (SEM) were used to characterize the nanoparticle size, as shown in Figure S1. The size of the nanoparticles measured by both methods was approximately 230 nm, and the nanoparticles were reasonably monodispersed.

2.3. ALD of Metal Oxides on Silica Nanoparticles. ALD of TiO_2 and $CaCO_3$ on SiO_2 nanoparticles was performed using a home-built ALD instrument that has been described previously.[27,28] $TiCl_4$ (Sigma-Aldrich, 99.9%) and bis(2,2,6,6-tetramethyl-3,5-heptanedionato)calcium ($Ca(TMHD)_2$, Strem Chemicals, 97%) were used as the Ti and Ca precursors, respectively. For each TiO_2 ALD cycle, the nanoparticles were evacuated and then exposed to $TiCl_4$ vapor at 423 K for 3 min, followed by oxidation in humid air at the same temperature for 6 min for ligand removal. For each $CaCO_3$ ALD cycle, the evacuated nanoparticles were exposed to $Ca(TMHD)_2$ vapor at 523 K for 10 min, followed by calcination at 773 K for 10 min. Eight ALD cycles of TiO_2 and 10 ALD cycles of $CaCO_3$ were performed to achieve complete coverage on SiO_2 nanoparticles.[16]

2.4. Temperature-Programmed Desorption of 2-Propanol. Temperature-programmed desorption (TPD) of 2-propanol was performed to probe the surface coverage of the ALD films on the SiO_2 nanoparticles. It has been reported that 2-propanol can react with the silanol groups of SiO_2 and form silyl-isopropyl ether species that desorb as propene at 770 K.[29,30] Therefore, the absence of a propene peak at 770 K in the TPD results can provide evidence of the complete coverage of ALD films. In a TPD measurement, the samples

https://doi.org/10.1021/acs.macromol.4c00823
Macromolecules 2024, 57, 8554−8561

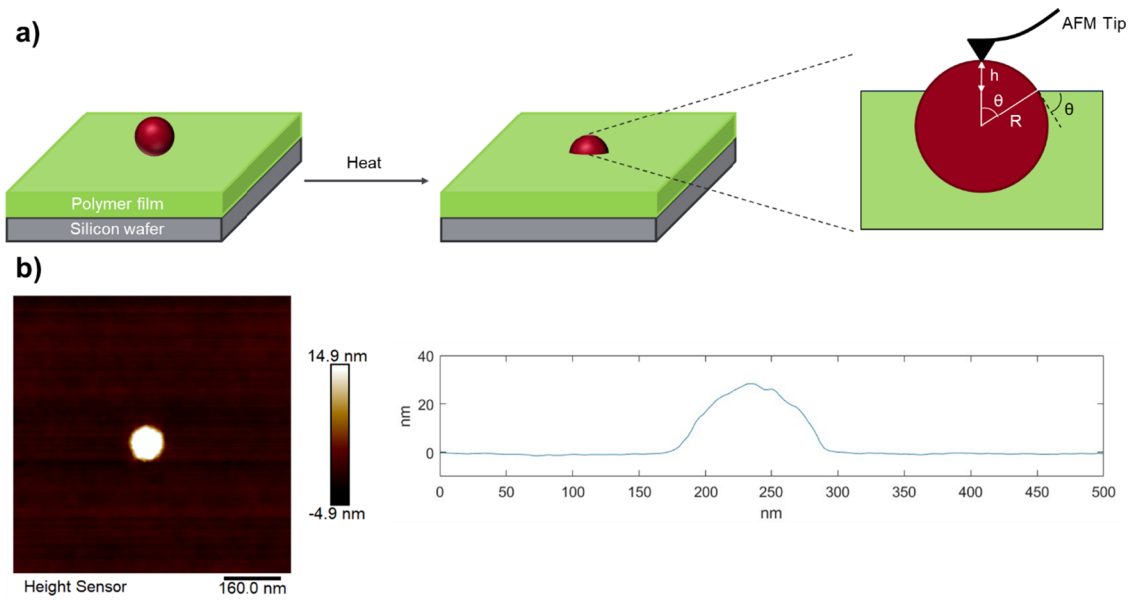

Figure 1. (a) Schematic illustration showing the measurement of the polymer−nanoparticle contact angle, (b) measuring the vertical distance between the top of the 226 nm SiO_2 NP and the 88,000 g/mol PS interface from 2D height sensor topography of NPs equilibrated at the polymer−air interface obtained via AFM.

were preheated to 823 K under evacuation, followed by exposure of 2-propanol vapor at 298 K. The samples were then heated from 298 to 823 at 10 K/min while measuring the desorbing species using a mass spectrometer (Stanford Research Systems, RGA-100).

2.5. Alkyl Silanization of Silica Nanoparticles. The silica nanoparticles were modified with an alkyl silane (i.e., octadecyltrimethoxysilane (C18-silane)) to increase their hydrophobicity. Specifically, the as-synthesized SiO_2 nanoparticles were dispersed in 35 mL of ethanol in a 50 mL centrifuge tube. Then, the particle suspension was added with 7 mL of ammonium hydroxide (28−30 wt %) followed by sonication to increase the dispersion of particles. Finally, 7 mL of diluted C18-silane in chloroform (10 vol %) was added, and the centrifuge tube was placed on a tube revolver rotator to proceed with the reaction. After 30 min, the C18-silane modified SiO_2 nanoparticles were washed three times with ethanol.[31,32]

2.6. Measurement of Polymer−Nanoparticle Contact Angle. Polymer thin films with a thickness of >500 nm were spin-coated on top of clean silicon wafers. A dilute suspension of the nanoparticles of 0.1 wt % was made in ethanol, which was then flow-coated on top of the polymer film to make a sparse coating (Figure S4). The sample was heated above the glass-transition or melting point of the polymer to 423 K for more than 10 days to allow the nanoparticles to equilibrate at the polymer−air interface. Subsequently, the height of the nanoparticle above the polymer−air interface, h, was measured at room temperature using AFM. The polymer−nanoparticle contact angle was then determined using the following equation:

$$\cos\theta = 1 - \frac{h}{R} \tag{2}$$

where R is the nanoparticle radius. The value of R was obtained from size characterization of the nanoparticles using DLS and SEM imaging, as shown in Figure S1. The samples with PE and hPCOE were heated in a chamber under a nominal steady N_2 flow to suppress the degradation of the polymer film. All other samples were heated in an oven under ambient conditions.

3. RESULTS AND DISCUSSION

Polymer−nanoparticle contact angles are directly determined by equilibrating nanoparticles at the planar polymer−air interface and subsequently measuring the height of the nanoparticle that protrudes out of the interface using AFM at room temperature as depicted in Figure 1 (see Section 2 for details). Based on the size of the nanoparticles, the polymer−nanoparticle contact angle can be determined using eq 2. A particle size of approximately 230 nm is chosen for the experiments because using particles <100 nm would amplify particle height measurement errors in determining the contact angles.

3.1. Polarizability Difference between PS and PE Affects Their Contact Angles on Metal Oxides. To determine the contact angle of a polymer on the SiO_2 nanoparticle, it is critical that the nanoparticle reaches its equilibrium contact angle during the annealing step. Previous studies on contact line aging of colloidal particles at oil−water interfaces have shown that the nanoparticle trajectories at the interface have a logarithmic dependence with time, implying that it could take a long time for colloidal particles to reach equilibrium asymptotically at the interface.[33] Studies have also shown enhanced surface mobility of polymer chains compared to bulk in polymer thin films near its glass-transition temperature.[34−36] To circumvent these complexities, the samples are heated at temperatures far above the glass-transition temperature of PS and melting points of PE and PCOE for long durations. As shown in Figure 2, SiO_2 nanoparticles equilibrate at the PE−air interface at 423 K within 7 days of heating. To ensure complete equilibration of the nanoparticles, we subjected all samples to heating for over 10 days prior to conducting contact angle measurements. While the equilibration time could potentially be shortened by heating the samples at higher temperatures, one should be mindful of polymer degradation at high temperatures. The samples with PE are heated under a N_2 purge to prevent polymer degradation. The IR spectra of the polymers are evaluated before and after the annealing process to confirm the absence of polymer degradation (Figure S5).

The equilibration of the nanoparticle at the polymer−air interface is governed by minimization of the surface energy of the system.[37] The total change in surface energy of the system (ΔE) is given by

https://doi.org/10.1021/acs.macromol.4c00823
Macromolecules 2024, 57, 8554−8561

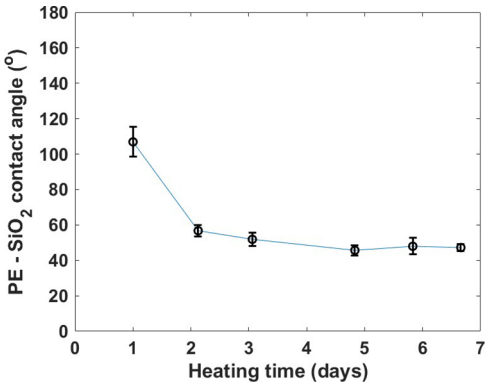

Figure 2. Contact angle evolution of 78,000 g/mol PE on 226 nm SiO_2 nanoparticles at 423 K.

$$\Delta E = E_{SL} + E_{SV} + E_{LV-NP} - E_{LV-noNP}$$

$$\Delta E = \gamma_{SL} 2\pi R^2 (1 + \cos\theta) + \gamma_{SV} 2\pi R^2 (1 - \cos\theta) - \gamma_{LV} \pi R^2 \sin^2\theta \quad (3)$$

where γ is the surface tension between two phases; S, L, and V refer to the solid, liquid, and vapor (or air) phases, respectively; NP refers to nanoparticle; R is the radius of the nanoparticle; and θ is the polymer−nanoparticle contact angle as shown in Figure 1a. The minimum total surface energy is obtained when

$$\cos\theta = \frac{\gamma_{SV} - \gamma_{SL}}{\gamma_{LV}} \quad (4)$$

which will be different for different polymer−nanoparticle pairs. The nanoparticle equilibration at the polymer interface is primarily driven by interfacial forces, and the prolonged heating of the samples allows for complete equilibration of the nanoparticles.

To explore the impact of nanoparticle surface chemistry and the structure of nonpolar polymers on the contact angle, we modify the surface of SiO_2 nanoparticles by coating them with various inorganic materials via ALD and select two nonpolar polymers with distinct polarizabilities. ALD enables the atomic-level precise deposition of diverse inorganic materials on the surfaces of nanoparticles and nanoporous materials without changing their size. TiO_2 and $CaCO_3$ represent common inorganic materials that are used as catalyst supports or inorganic fillers for nanocomposites. We chose to do ALD of TiO_2 and $CaCO_3$ on spherical SiO_2 nanoparticles to maintain the consistency of our work by using one type of monodispersed particles for all of the measurements. We confirm the full coverage of SiO_2 with a new material using TPD of 2-propanol. This involves allowing 2-propanol to adsorb onto the surface of the nanoparticles, followed by heating them and tracking the desorbed species using mass spectrometry.

As shown in Figure 3, some hydrogen-bonded, weakly adsorbed 2-propanol leave each of the surfaces unreacted below approximately 500 K. Differences in the specific surface chemistries are observed by following the reaction products. SiO_2 has a characteristic propene desorption peak close to 800 K that is due to the decomposition of isopropyl-silyl ethers that form by the reaction of the alcohol with exposed silanols. However, for nanoparticles coated with TiO_2, propene is

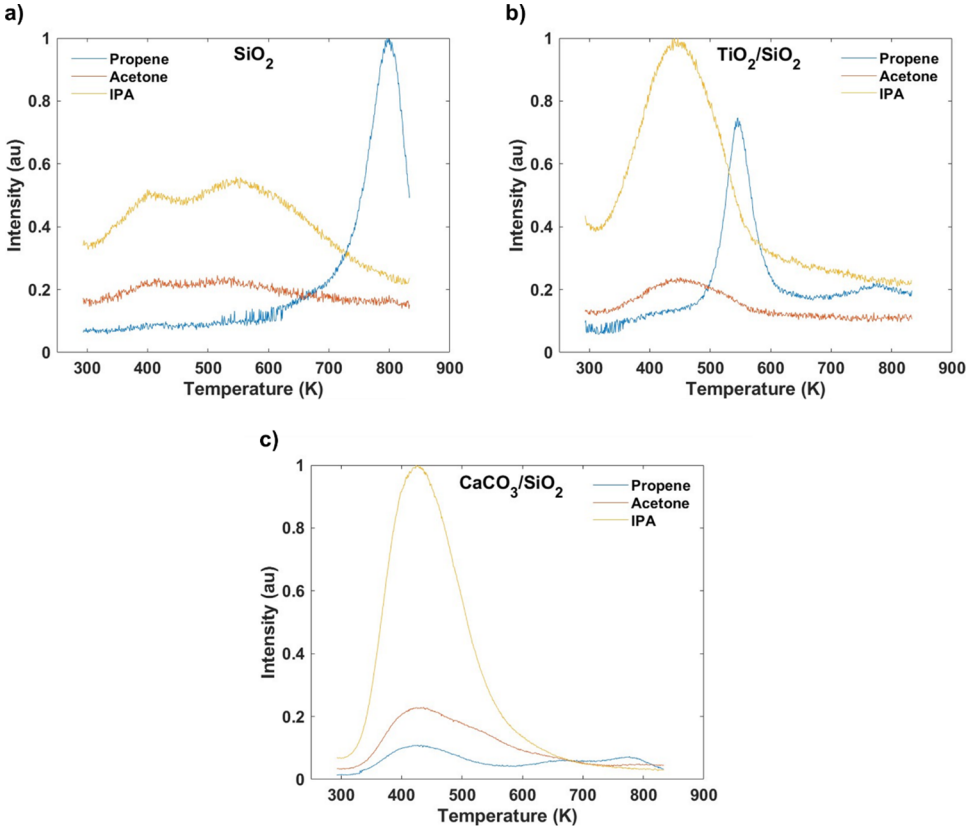

Figure 3. TPD of 2-propanol for (a) SiO_2, (b) TiO_2-coated, and (c) $CaCO_3$-coated nanoparticles.

https://doi.org/10.1021/acs.macromol.4c00823
Macromolecules 2024, 57, 8554−8561

formed at 550 K due to the Lewis-acid character of TiO_2. The absence of an 800 K peak confirms complete surface coverage of the silica surface. For nanoparticles coated with $CaCO_3$, only unreacted 2-propanol is observed leaving the surface, with the absence of the 800 K propene peak confirming that the silica surface is completely covered by $CaCO_3$.

PE and PS are selected as model nonpolar polymers due to their widespread use and distinct characteristics. PE is highly nonpolarizable, while PS's phenyl pendant group offers considerable polarizability, providing a contrast in polymer properties. For comparison, styrene has a polarizability (α) of 1.28×10^{-23} cm^3,[38] while that for ethylene is 0.42×10^{-23} cm^3.[39] This comparative approach allows us to systematically assess how variations in the structure of nonpolar polymers and the surface chemistry of nanoparticles influence the contact angle, aiming to bridge the knowledge gap in polymer−nanoparticle interactions.

A smaller contact angle indicates stronger interactions between the polymer and nanoparticles, and vice versa. Contact angles of PE and PS on SiO_2, TiO_2, and $CaCO_3$ in Figure 4 show that PS has slightly stronger interactions with

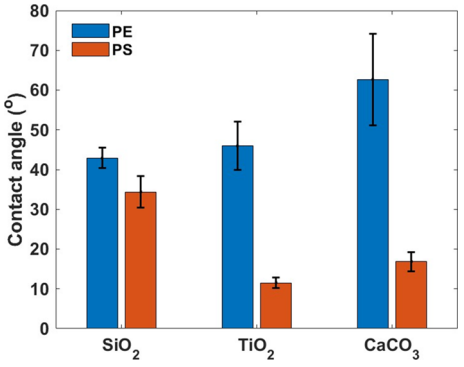

Figure 4. Contact angles of PE78k and PS88k on SiO_2, TiO_2-coated, and $CaCO_3$-coated nanoparticles.

SiO_2 as compared to PE, as evidenced by the difference in the contact angle from 45 to 34°; in contrast, PS has much stronger interactions with TiO_2 and $CaCO_3$ compared to PE as the contact angles of PS on TiO_2 and $CaCO_3$ are 12 and 17°, respectively, while the corresponding contact angles of PE are 46 and 63°. The differences in interactions between PS and PE can be attributed to the presence of polarizable aromatic rings in PS leading to stronger electrostatic interactions with the polar metal oxide-covered nanoparticles.

3.2. Presence of Double Bonds in PCOE Leads to Stronger Interactions with Metal Oxides Compared to hPCOE. A potential way to upcycle chemically robust polyolefins such as PE is by incorporating double bonds in the polymer backbone through partial dehydrogenation.[40−42] These double bonds can then be reacted to incorporate various functional groups or side chains into the polymer backbone, giving them valuable functionality such as high adhesivity and toughness. For this purpose, we use PCOE, which has one C=C double bond per every 8-carbon repeat unit, as a model polymer for partially dehydrogenated PE and fully hydrogenated polycyclooctene (hPCOE) as an analogue for PE. For catalytic dehydrogenation of PE using heterogeneous catalysis, the interactions between the reactant and product polymers and the solid catalyst particles are critical in determining the efficacy of the catalyst. Moreover, these two polymers represent two highly nonpolar polymers with a very small difference in their polarizability. It is unclear whether inorganic solid surfaces can interact differently with two polymers with such a small difference in the structure.

To probe this, we measure the contact angles of PCOE and hPCOE on SiO_2, TiO_2, and $CaCO_3$. The PCOE samples are heated at 373 K because of their lower melting point of ∼330 K (Figure S7), while the hPCOE samples are heated at 423 K. Interestingly, in all three cases, PCOE has lower contact angles with the inorganic nanoparticles by about 10−20° compared to hPCOE, as shown in Figure 5. This demonstrates that even

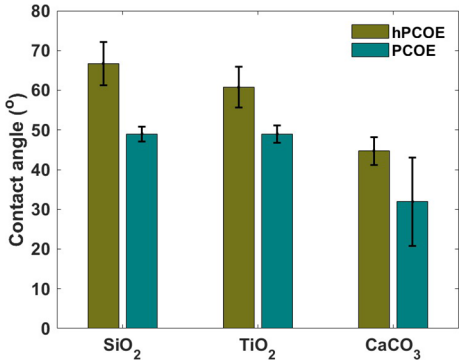

Figure 5. Contact angles of PCOE and hPCOE on SiO_2, TiO_2-coated, and $CaCO_3$-coated nanoparticles.

small differences in the structure of the polymer can lead to appreciable differences in their interaction strength with inorganic solid surfaces. We also observe that PCOE has similar interactions with both SiO_2 and TiO_2 due to comparable contact angle values of 49° but slightly stronger interactions with $CaCO_3$, as evidenced by a decrease in the contact angle to 32°. The differences in interaction strength between PCOE and hPCOE with inorganic solid surfaces can be attributed to the presence of more polarizable C=C bonds in the PCOE molecules compared to the C−C bonds in hPCOE.

While the differences in contact angle between PS and PE on TiO_2- and $CaCO_3$-coated nanoparticles are significant, the same cannot be said for hPCOE and PCOE. We do not fully understand why that is the case but hypothesize that there could be additional interactions of the metal oxides with PS that are absent for PCOE. We also observe that the contact angles of both PE and hPCOE on SiO_2 nanoparticles and TiO_2-coated nanoparticles are similar. However, the same cannot be said for $CaCO_3$-coated nanoparticles. The contact angle of PE on $CaCO_3$-coated nanoparticles is greater than those on SiO_2 and TiO_2 but that of hPCOE is lower than those on SiO_2 and TiO_2. While we do not fully understand the reason for this discrepancy, we highlight that the PE and hPCOE polymers are synthesized by different reaction mechanisms, which could result in minor variations in their molecular composition. There is evidence of such minor differences in the IR spectra of the two polymers (Figure S6). The synthesized hPCOE has very small amounts of C−O bonds present in the molecules, as evidenced by the small peak at ∼1100 cm^{-1}. The hPCOE is synthesized by the hydrogenation of PCOE by a diimide reaction, and the PCOE is synthesized by ring-opening metathesis polymerization of cis-cyclooctene, as described in the Supporting Information. The hPCOE polymer can be considered an analogue for high-

https://doi.org/10.1021/acs.macromol.4c00823
Macromolecules 2024, 57, 8554−8561

density polyethylene. On the other hand, the PE polymer is made by the hydrogenation of polybutadiene, rich in 1,4-microstructure, which itself is synthesized by living anionic polymerization of butadiene in a nonpolar solvent. There will likely have been some 1,2-addition of the 1,4-butadiene monomers during anionic synthesis. After hydrogenation, this would lead to the PE chains having some ethyl pendant groups. This would make the PE polymer more similar to linear low-density polyethylene. This is further supported by melting points of the two polymers, with PE having a T_m of 385 K[43] and hPCOE having a T_m of ~403 K (Figure S7). The molecular weights and polydispersity of the two polymers are also different, with PE having a molecular weight of 78,000 g/mol ($Đ$ = 1.05), while hPCOE has a molecular weight of 52,000 g/mol ($Đ$ = 1.62). There could also be differences in crystallinity between the PE and hPCOE polymers, which we did not investigate in this study. Further analysis would be necessary to identify the exact reason for this discrepancy.

3.3. Alkyl Silanization of SiO_2 NPs to Make Their Surface Nonpolar Reverses Relative Interaction Strengths between PCOE and hPCOE. Due to the difference in polarizability between PCOE and hPCOE and the polar nature of the metal oxide nanoparticles, PCOE interacts with these surfaces more favorably than hPCOE. However, to enable efficient dehydrogenation of PE, it is critical that the reactant has stronger interactions with the catalyst supports than the product; otherwise, the product would preferably interact with the catalyst and inhibit dehydrogenation of the reactant. To reverse this trend, we hypothesize that making the nanoparticle surface nonpolar could change the relative strength of interactions with the two polymers. Hence, we silanize SiO_2 nanoparticles with octadecyltrimethoxysilane (OTS), which has an 18-carbon-long alkyl chain to make the surface of the nanoparticles nonpolar. The silanization reaction is performed for 30 min to ensure complete silanization (Figure S8).

Upon measuring the contact angles of PCOE and hPCOE on the alkyl silanized nanoparticles, we find that it is indeed possible to reverse the relative strength of interactions between the polymers and the nanoparticles. As shown in Figure 6,

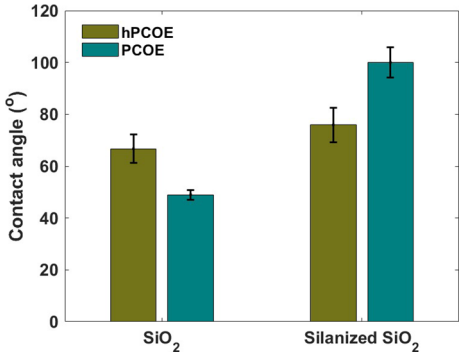

Figure 6. Contact angles of PCOE and hPCOE on SiO_2 and octadecyl-silanized SiO_2 nanoparticles.

PCOE has a smaller contact angle with SiO_2 nanoparticles compared to hPCOE but has a larger contact angle with the alkyl silanized nanoparticles compared to hPCOE. It is also worth noting that the strength of interactions (or contact angle) of hPCOE with both the SiO_2 nanoparticles and the alkyl silanized nanoparticles is comparable due to the absence of polarizable groups in hPCOE, and hence, there is an absence of electrostatic interactions with both the SiO_2 and the alkyl silanized nanoparticles. This is evidenced by the fact that upon alkyl silanization of the SiO_2 nanoparticles, the contact angle of PCOE increases significantly from 49 to 100°, whereas that of hPCOE increases by only about 9° from 67 to 76°. In the context of catalyst design, alkyl silanization of catalytic supports could potentially be an effective way of synthesizing efficacious heterogeneous catalysts for the dehydrogenation of polyolefins.

4. CONCLUSIONS

In this study, we modulate the interaction strength between nonpolar polymers and nanoparticles by modifying the surface chemistry of the nanoparticles through ALD and alkyl silanization. We observe that the polarizability of the polymers plays a key role in determining the strength of interactions with nanoparticles with varying compositions. There are significant differences in contact angles of PS and PE on metal oxide-coated nanoparticles due to PS being more polarizable compared to PE. We also observe that PCOE, which is slightly more polarizable compared to hPCOE due to the presence of C=C bonds, consistently has stronger interactions with metal oxides in comparison to hPCOE. Further studies would be necessary to understand the quantitative relationship between the polymer−nanoparticle contact angle and the polarizability of nonpolar polymers based on a theoretical model. However, the direct measurement of the polymer−nanoparticle contact angle is a big step toward quantifying the strength of interactions between them and understanding how small differences in polarizability of nonpolar polymers can lead to significantly different interaction strengths. Finally, the relative strength of interactions between PCOE and hPCOE with the nanoparticles could be modulated by making the nanoparticle surface nonpolar via alkyl silanization. This leads to a reversal of the relative interaction strengths, with PCOE having weaker interactions with the alkyl silanized nanoparticles compared to hPCOE. This approach provides a possible way to make efficacious heterogeneous catalysts for polymer upcycling reactions, where the product polymer is more polarizable than the reactant polymer. Effective quantification of polymer−nanoparticle interactions via contact angle measurements and the ability to modulate these interactions will enable the design of polymer nanocomposites with desired morphologies and properties. For polymer upcycling reactions involving heterogeneous catalysts, significant differences in polymer−solid interactions can potentially enable the selective conversion of polymers without the need for prior separation from complex feed streams, making the process more sustainable and energy efficient.

■ ASSOCIATED CONTENT

Supporting Information

The Supporting Information is available free of charge at https://pubs.acs.org/doi/10.1021/acs.macromol.4c00823.

Size characterization of silica nanoparticles; synthesis of polycyclooctene; hydrogenation of polycyclooctene by diimide reduction; sample preparation; FTIR analysis and thermal characterization of polymers; and AFM analysis PDF

https://doi.org/10.1021/acs.macromol.4c00823
Macromolecules 2024, 57, 8554−8561

AUTHOR INFORMATION

Corresponding Author

Daeyeon Lee − *Department of Chemical & Biomolecular Engineering, University of Pennsylvania, Philadelphia, Pennsylvania 19104, United States;* orcid.org/0000-0001-6679-290X; Email: daeyeon@seas.upenn.edu

Authors

Anirban Majumder − *Department of Chemical & Biomolecular Engineering, University of Pennsylvania, Philadelphia, Pennsylvania 19104, United States*

Anne N. Radzanowski − *Department of Polymer Science & Engineering, University of Massachusetts, Amherst, Massachusetts 01003, United States;* orcid.org/0000-0001-6453-3103

Ching-Yu Wang − *Department of Chemical & Biomolecular Engineering, University of Pennsylvania, Philadelphia, Pennsylvania 19104, United States*

Yijiang Mu − *Department of Chemical & Biomolecular Engineering, University of Pennsylvania, Philadelphia, Pennsylvania 19104, United States*

E. Bryan Coughlin − *Department of Polymer Science & Engineering, University of Massachusetts, Amherst, Massachusetts 01003, United States;* orcid.org/0000-0001-7065-4366

Raymond J. Gorte − *Department of Chemical & Biomolecular Engineering, University of Pennsylvania, Philadelphia, Pennsylvania 19104, United States;* orcid.org/0000-0003-0879-715X

John M. Vohs − *Department of Chemical & Biomolecular Engineering, University of Pennsylvania, Philadelphia, Pennsylvania 19104, United States;* orcid.org/0000-0002-8283-5241

Complete contact information is available at: https://pubs.acs.org/10.1021/acs.macromol.4c00823

Author Contributions

The manuscript was written through contributions of all authors. All authors have given approval to the final version of the manuscript.

Funding

DOE BES (DE-SC0022238), Vagelos Institute for Energy Science and Technology Graduate Student Fellowship.

Notes

The authors declare no competing financial interest.

ACKNOWLEDGMENTS

The authors gratefully acknowledge funding by DOE BES (DE-SC0022238) and the Vagelos Institute for Energy Science and Technology Graduate Student Fellowship for supporting this work. This work was carried out in part at the Singh Center for Nanotechnology at the University of Pennsylvania.

ABBREVIATIONS

AFM:atomic force microscopy; SEM:scanning electron microscopy; DLS:dynamic light scattering; PCOE:polycyclooctene; hPCOE:fully hydrogenated polycyclooctene; PE:polyethylene; PS:polystyrene; NP:nanoparticle; TPD:temperature-programmed desorption; SiO_2:silica; TiO_2:titania; $CaCO_3$:calcium carbonate

REFERENCES

(1) Lee, D. W.; Yoo, B. R. Advanced Silica/Polymer Composites: Materials and Applications. *J. Ind. Eng. Chem.* **2016**, *38*, 1−12.

(2) Venkatesh, R. B.; Manohar, N.; Qiang, Y.; Wang, H.; Tran, H. H.; Kim, B. Q.; Neuman, A.; Ren, T.; Fakhraai, Z.; Riggleman, R. A.; Stebe, K. J.; Turner, K.; Lee, D. Polymer-Infiltrated Nanoparticle Films Using Capillarity-Based Techniques: Toward Multifunctional Coatings and Membranes. *Annu. Rev. Chem. Biomol. Eng.* **2021**, *12* (1), 411−437.

(3) Qiang, Y.; Turner, K. T.; Lee, D. Role of Polymer−Nanoparticle Interactions on the Fracture Toughness of Polymer-Infiltrated Nanoparticle Films. *Macromolecules* **2023**, *56* (1), 122−135.

(4) Qiang, Y.; Pande, S. S.; Lee, D.; Turner, K. T. The Interplay of Polymer Bridging and Entanglement in Toughening Polymer-Infiltrated Nanoparticle Films. *ACS Nano* **2022**, *16* (4), 6372−6381.

(5) Liu, J.; Gao, Y.; Cao, D.; Zhang, L.; Guo, Z. Nanoparticle Dispersion and Aggregation in Polymer Nanocomposites: Insights from Molecular Dynamics Simulation. *Langmuir* **2011**, *27* (12), 7926−7933.

(6) Pandav, G.; Pryamitsyn, V.; Ganesan, V. Interactions and Aggregation of Charged Nanoparticles in Uncharged Polymer Solutions. *Langmuir* **2015**, *31* (45), 12328−12338.

(7) Kulshreshtha, A.; Jayaraman, A. Dispersion and Aggregation of Polymer Grafted Particles in Polymer Nanocomposites Driven by the Hardness and Size of the Grafted Layer Tuned by Attractive Graft−Matrix Interactions. *Macromolecules* **2020**, *53* (4), 1302−1313.

(8) Amgoune, A.; Krumova, M.; Mecking, S. Nanoparticle-Supported Molecular Polymerization Catalysts. *Macromolecules* **2008**, *41* (22), 8388−8396.

(9) Tennakoon, A.; Wu, X.; Paterson, A. L.; Patnaik, S.; Pei, Y.; LaPointe, A. M.; Ammal, S. C.; Hackler, R. A.; Heyden, A.; Slowing, I. I.; Coates, G. W.; Delferro, M.; Peters, B.; Huang, W.; Sadow, A. D.; Perras, F. A. Catalytic upcycling of High-Density Polyethylene via a Processive Mechanism. *Nat. Catal.* **2020**, *3* (11), 893−901.

(10) Zhao, T. Y.; Meirow, M.; Tennakoon, A.; Wu, X.; Paterson, A. L.; Qi, L.; LaPointe, A. M.; Lamb, J. V.; Kobayashi, T.; Delferro, M.; Sadow, A. D.; Huang, W.; Luijten, E.; Perras, F. A. Mechanistic Insights into Processive Polyethylene Hydrogenolysis through *In Situ* NMR. *Macromolecules* **2023**, *56* (11), 4287−4295.

(11) Johnston, K.; Harmandaris, V. Hierarchical Simulations of Hybrid Polymer−Solid Materials. *Soft Matter* **2013**, *9* (29), 6696.

(12) Chang, A.; Babhadiashar, N.; Barrett-Catton, E.; Asuri, P. Role of Nanoparticle−Polymer Interactions on the Development of Double-Network Hydrogel Nanocomposites with High Mechanical Strength. *Polymers* **2020**, *12* (2), 470.

(13) Sadeghi, A.; PourEskandar, S.; Askari, E.; Akbari, M. Polymeric Nanoparticles and Nanogels: How Do They Interact with Proteins? *Gels* **2023**, *9* (8), 632.

(14) Yang, E.; Ivancic, R. J. S.; Lin, E. Y.; Riggleman, R. A. Effect of Polymer−Nanoparticle Interaction on Strain Localization in Polymer Nanopillars. *Soft Matter* **2020**, *16* (37), 8639−8646.

(15) Ren, T.; Wang, C.-Y.; Huang, R.; Deng, C.; Xu, Y.; Majumder, A.; Ra, J.; Shen, K.; Vohs, J. M.; De Pablo, J. J.; Gorte, R. J.; Lee, D. Understanding Polymer-Porous Solid Interactions Based on Small Gas Molecule Adsorption Behavior. *Chem. Eng. J.* **2023**, *473*, No. 145220.

(16) Ren, T.; Huang, R.; Gorte, R. J.; Lee, D. Modulating Interactions between Molten Polystyrene and Porous Solids Using Atomic Layer Deposition. *Langmuir* **2021**, *37* (49), 14520−14526.

(17) Seemann, R.; Jacobs, K.; Blossey, R. Polystyrene Nanodroplets *. *J. Phys.: Condens. Matter* **2001**, *13* (21), 4915−4923.

(18) McBride, S. P.; Law, B. M. Influence of Line Tension on Spherical Colloidal Particles at Liquid-Vapor Interfaces. *Phys. Rev. Lett.* **2012**, *109* (19), No. 196101.

(19) Arnaudov, L. N.; Cayre, O. J.; Cohen Stuart, M. A.; Stoyanov, S. D.; Paunov, V. N. Measuring the Three-Phase Contact Angle of Nanoparticles at Fluid Interfaces. *Phys. Chem. Chem. Phys.* **2010**, *12* (2), 328−331.

(20) Fastow, E.; Chethalen, R. J.; Coughlin, E. B.; Winey, K. I. Thiol-Ene Click Chemistry Incorporates Carboxylic Acid-Terminated Alkane Pendants on Polycyclooctene to Tune Properties. *Giant* **2024**, *17*, No. 100231.
(21) Chethalen, R. J.; Fastow, E. J.; Coughlin, E. B.; Winey, K. I. Thiol−Ene Click Chemistry Incorporates Hydroxyl Functionality on Polycyclooctene to Tune Properties. *ACS Macro Lett.* **2023**, *12* (1), 107−112.
(22) Hillmyer, M. A.; Nguyen, S. T.; Grubbs, R. H. Utility of a Ruthenium Metathesis Catalyst for the Preparation of End-Functionalized Polybutadiene. *Macromolecules* **1997**, *30* (4), 718−721.
(23) Zhang, J.; Matta, M. E.; Martinez, H.; Hillmyer, M. A. Precision Vinyl Acetate/Ethylene (VAE) Copolymers by ROMP of Acetoxy-Substituted Cyclic Alkenes. *Macromolecules* **2013**, *46* (7), 2535−2543.
(24) Hahn, S. F. An Improved Method for the Diimide Hydrogenation of Butadiene and Isoprene Containing Polymers. *J. Polym. Sci. Part Polym. Chem.* **1992**, *30* (3), 397−408.
(25) Buggy, N. C.; Du, Y.; Kuo, M.-C.; Ahrens, K. A.; Wilkinson, J. S.; Seifert, S.; Coughlin, E. B.; Herring, A. M. A Polyethylene-Based Triblock Copolymer Anion Exchange Membrane with High Conductivity and Practical Mechanical Properties. *ACS Appl. Polym. Mater.* **2020**, *2* (3), 1294−1303.
(26) Stöber, W.; Fink, A.; Bohn, E. Controlled Growth of Monodisperse Silica Spheres in the Micron Size Range. *J. Colloid Interface Sci.* **1968**, *26* (1), 62−69.
(27) Onn, T.; Küngas, R.; Fornasiero, P.; Huang, K.; Gorte, R. Atomic Layer Deposition on Porous Materials: Problems with Conventional Approaches to Catalyst and Fuel Cell Electrode Preparation. *Inorganics* **2018**, *6* (1), 34.
(28) Wang, C.-Y.; Ferko, B. T.; Shen, K.; Winey, K. I.; Vohs, J. M.; Gorte, R. J. Determination of Film Thicknesses of Metal Oxides Prepared by Atomic Layer Deposition on SBA-15. *Microporous Mesoporous Mater.* **2024**, *366*, No. 112945.
(29) Huang, R.; Cheng, Y.; Ji, Y.; Gorte, R. J. Atomic Layer Deposition for Preparing Isolated Co Sites on SiO2 for Ethane Dehydrogenation Catalysis. *Nanomaterials* **2020**, *10* (2), 244.
(30) Wang, C.-Y.; Kwon, O.; Gorte, R. J.; Vohs, J. M. Synthesis of High-Surface Area Tungstated Zirconia by Atomic Layer Deposition on Mesoporous Silica. *Microporous Mesoporous Mater.* **2022**, *335*, No. 111821.
(31) Mu, Y.; Tran, H.; Xiang, Z.; Majumder, A.; Hsu, E.; Steager, E.; Koo, H.; Lee, D. Spiky Magnetic Microparticles Synthesized from Microrod-Stabilized Pickering Emulsion. *Small* **2024**, No. 2402292.
(32) Yi, G.-R.; Manoharan, V. N.; Michel, E.; Elsesser, M. T.; Yang, S.-M.; Pine, D. J. Colloidal Clusters of Silica or Polymer Microspheres. *Adv. Mater.* **2004**, *16* (14), 1204−1208.
(33) Kaz, D. M.; McGorty, R.; Mani, M.; Brenner, M. P.; Manoharan, V. N. Physical Ageing of the Contact Line on Colloidal Particles at Liquid Interfaces. *Nat. Mater.* **2012**, *11* (2), 138−142.
(34) Fakhraai, Z.; Forrest, J. A. Measuring the Surface Dynamics of Glassy Polymers. *Science* **2008**, *319* (5863), 600−604.
(35) Ilton, M.; Qi, D.; Forrest, J. A. Using Nanoparticle Embedding to Probe Surface Rheology and the Length Scale of Surface Mobility in Glassy Polymers. *Macromolecules* **2009**, *42* (18), 6851−6854.
(36) Chai, Y.; Salez, T.; McGraw, J. D.; Benzaquen, M.; Dalnoki-Veress, K.; Raphaël, E.; Forrest, J. A. A Direct Quantitative Measure of Surface Mobility in a Glassy Polymer. *Science* **2014**, *343* (6174), 994−999.
(37) Guzmán, E.; Ortega, F.; Rubio, R. G. Forces Controlling the Assembly of Particles at Fluid Interfaces. *Langmuir* **2022**, *38* (44), 13313−13321.
(38) Zhang, X.; Wang, G.; Luo, B.; Tan, F.; Bland, S. N.; Zhao, J.; Sun, C.; Liu, C. Refractive Index and Polarizability of Polystyrene under Shock Compression. *J. Mater. Sci.* **2018**, *53* (17), 12628−12640.
(39) Olney, T. N.; Cann, N. M.; Cooper, G.; Brion, C. E. Absolute Scale Determination for Photoabsorption Spectra and the Calculation of Molecular Properties Using Dipole Sum-Rules. *Chem. Phys.* **1997**, *223* (1), 59−98.
(40) Conk, R. J.; Hanna, S.; Shi, J. X.; Yang, J.; Ciccia, N. R.; Qi, L.; Bloomer, B. J.; Heuvel, S.; Wills, T.; Su, J.; Bell, A. T.; Hartwig, J. F. Catalytic Deconstruction of Waste Polyethylene with Ethylene to Form Propylene. *Science* **2022**, *377* (6614), 1561−1566.
(41) Arroyave, A.; Cui, S.; Lopez, J. C.; Kocen, A. L.; LaPointe, A. M.; Delferro, M.; Coates, G. W. Catalytic Chemical Recycling of Post-Consumer Polyethylene. *J. Am. Chem. Soc.* **2022**, *144* (51), 23280−23285.
(42) Ray, A.; Zhu, K.; Kissin, Y. V.; Cherian, A. E.; Coates, G. W.; Goldman, A. S. Dehydrogenation of Aliphatic Polyolefins Catalyzed by Pincer-Ligated Iridium Complexes. *Chem. Commun.* **2005**, *27*, 3388.
(43) Ren, T. *Understanding and Controlling Behavior of Polymers in Porous Media*; Doctoral dissertation, University of Pennsylvania, 2023.

https://doi.org/10.1021/acs.macromol.4c00823
Macromolecules 2024, 57, 8554−8561